Alexandria Engineering Journal (2011) **50**, 269–282

Alexandria University

Alexandria Engineering Journal

www.elsevier.com/locate/aej
www.sciencedirect.com

ORIGINAL ARTICLE

Numerical simulation of double-diffusive natural convective flow in an inclined rectangular enclosure in the presence of magnetic field and heat source, part A: Effect of Rayleigh number and inclination angle

Mohamed A. Teamah *, Ahmed F. Elsafty, Mahmoud Z. Elfeky, Enass Z. El-Gazzar

Mechanical Engineering Department, College of Engineering and Technology, Arab Academy for Science Technology and Maritime Transport, Egypt

Received 13 January 2010; accepted 19 May 2010
Available online 6 October 2011

KEYWORDS

Double-diffusive flow;
Heat and mass transfer;
Magnetic field;
Heat generation;
Inclination;
Numerical solution

Abstract Double-diffusive convective flow in an inclined rectangular enclosure with the shortest sides being insulated and impermeable is investigated numerically. Constant temperatures and concentration are imposed along the longest sides of the enclosure. In addition, a uniform magnetic field is applied in a horizontal direction. Laminar regime is considered under steady state condition. The transport equations for continuity, momentum, energy and species transfer are solved using the finite volume technique. The validity of the numerical code used is ascertained and good agreement was found with published results. The numerical results are reported for the effect of thermal Rayleigh number on the contours of streamline, temperature, and concentration. In addition, results for the average Nusselt and Sherwood numbers are presented and discussed for various parametric conditions. This study was done for constant Prandtl number, Pr = 0.7, aspect ratio, $A = 2$, Lewis number, Le = 2, the buoyancy ratio, $N = 1$, Hartmann number, Ha = 10 and the dimensionless

* Corresponding author.
E-mail address: mteameh@aast.edu (M.A. Teamah).

Peer review under responsibility of Faculty of Engineering, Alexandria University.
doi:10.1016/j.aej.2010.05.001

Production and hosting by Elsevier

heat generation, $\Phi = 1$. Computations are carried out for Ra_T ranging from 10^3 to $5 * 10^5$ and inclination angle range of $0° \leqslant \gamma \leqslant 180°$.

Nomenclature

A	aspect ratio, H/L
B	magnetic induction, $Tesla = N/Am^2$
C	vapor concentration
c_h	concentrations at the left wall of the cavity
c_l	concentrations at the right wall of the cavity
C	dimensionless vapor concentration, $C = (c - c_l)/(c_h - c_l)$
C_p	specific heat at constant pressure
D	mass diffusivity
g	acceleration of gravity
h	heat transfer coefficient
h_s	solutal transfer coefficient
H	cavity height
k	fluid thermal conductivity
L	cavity width
Le	Lewis number, $Le = \alpha/D$
N	buoyancy ratio
Nu	average Nusselt number, $Nu = hL/k$
Nu_i	local Nusselt number
p	pressure
P	dimensionless pressure, $P = pL^2/\rho^*\alpha^2$
Pr	Prandtl number, $Pr = \nu/\alpha$
Q_o	heat generation or absorption coefficient, W/m^3 °C
Ra_S	solutal Rayleigh number, $Ra_S = Gr_S\ Pr$
Ra_T	thermal Rayleigh number, $Ra_T = Gr_T\ Pr$
Sh	average *Sherwood* number, $Sh = h_s\ L/D$
Sh_i	local Sherwood number
T	local temperature
T_c	cold wall temperature
T_h	hot wall temperature
ΔT	temperature difference
u	velocity components in x direction
v	velocity components in y direction
U	dimensionless velocity component in X direction
V	dimensionless velocity component in Y direction
x, y	dimensional coordinates
X, Y	dimensionless coordinates

Greek symbols

α	thermal diffusivity
β_T	coefficient of thermal expansion
β_S	coefficient of solutal expansion
Φ	dimensionless heat generation or absorption
θ	dimensionless temperature, $(T - T_c)/(T_h - T_c)$
μ	dynamic viscosity
ν	kinematics viscosity
ρ	local fluid density
ρ_o	fluid density at the bottom surface
ρ^*	dimensionless density, $NC - \theta$
ψ	dimensionless stream function
ψ_{max}	maximum dimensionless stream function
γ	inclination angle
σ	electrical conductivity

1. Introduction

Natural convection is of a great importance in many industrial applications. Application of natural convection in engineering can be found in the solar collectors, furnaces, building heating and cooling system, heat exchangers, and so on. Buoyancy-induced flow and heat transfer in enclosures have received considerable attention by many researches both experimentally and numerically. A good review was reported by de Vahl Davis [1].

Natural convection heat transfer induced by internal heat generation has recently received considerable attention because of numerous applications in geophysics and energy-related engineering problems. Such applications include heat removal from nuclear fuel debris, underground disposal of radioactive waste materials, storage of foodstuff, and exothermic chemical reactions in packed-bed reactor. Acharya and Goldstein [2] studied numerically a complicated inclined cavity with inner heat generation. Two Rayleigh numbers were introduced; internal Rayleigh number Ra_I which is based on the rate of heat generation and external Rayleigh number Ra_E which is based on the temperature difference. The study covered a range for Ra_I from 10^4 to 10^7, Ra_E from 10^3 to 10^6 and cavity inclination angle from 30° to 90°.

Also, Rahman and Sharif [3] studied numerically the same geometry with heated bottom and cooled top surfaces and insulated sides. In their study, both Ra_I and Ra_E were 2×10^5 and the aspect ratio ranged from 0.25 to 4. They found that for $Ra_E/Ra_I > 1$, the convective flow and heat transfer were almost the same as that in a cavity without internal heat generating fluid and they observed similar results as in Acharya and Goldstein [2].

Heat transfer in partially divided enclosures has received attention primarily due to its many applications such as the design of energy efficient building, reduction of heat loss from flat plate solar collectors, natural gas storage tanks, crystal manufacturing and metal solidification processes. AlAmiri et al. [4] studied numerically buoyancy-induced heat transfer in a partially divided square enclosure with protruding isothermal heater. Their study covered Rayleigh number in the range of $10^4 \leqslant Ra \leqslant 5 * 10^7$. Various pertinent parameters such as Rayleigh number, height of the heater, heater width,

and heater location were carried out to investigate the effect of the protruding heater on the heat transfer within the cavity.

In addition, Oztop and Bilgen [5] studied numerically heat transfer in a differentially heated, partitioned, square cavity containing heat generating fluid which adds an additional dynamic effect to overall convection characteristics. The authors illustrated that the cold partition decreased heat transfer within the enclosure and the heat reduction was gradually increased with increasing partition height and thickness. Moreover, heat transfer within the enclosure was also reduced significantly when the partition was closer to the hot or cold wall.

Magnetic damping is one of the effective means practiced in industry for thermally induced melt flow control. It is imitative from the interaction between an electrically conducting melt flow and an applied magnetic field to generate an opposing Lorentz force to the convective flows in the melt. The damping effect depends on the strength of the applied magnetic field and its orientation with respect to the convective flow direction. Substantial theoretical and numerical work, thus far, has appeared on magnetic damping for natural convection [6–14].

Double diffusive convection occurs in a wide range of fields such as Oceanography, Astrophysics, Geology, Biology, Chemical processes, Crystal growth, etc. The double-diffusive convection, which takes place when compositionally driven buoyant convection and thermally driven buoyant convection occur simultaneously, arises in a very wide range of fields such as Oceanography, Astrophysics, Chemical vapor transport process, Drying process, Crystal growth process, etc. Reviews on this subject can be found in the publications of Ostrach [15], Costa [16–17] and Nishimuraet al. [18]. Different enclosure geometries were studied in these researches including square, parallelogram and rectangular enclosures.

Chouikh et al. [19] studied numerically the natural convection flow resulting from the combined buoyancy effects of thermal and mass diffusion in an inclined glazing cavity with differentially heated side walls. The numerical approach endorsed the authors to analyze the complex natural convection flow situations arising in the inclined glazing cavity and to evaluate the effect of different parameters on the solar still performance.

Nithyadevi and Yang [20] studied numerically the effect of double-diffusive natural convection of water in a partially heated enclosure with Soret and Dufour coefficients around the density maximum. The right vertical wall has constant temperature while left vertical wall is partially heated. The concentration in right wall is maintained higher than left wall for case I, and concentration is lower in right wall than left wall for case II. The effect of the different parameters (thermal Rayleigh number, centre of the heating location, density inversion parameter, Buoyancy ratio number, Schmidt number, and Soret and Dufour coefficients) on the flow pattern and heat and mass transfer has been discussed.

Chamkha and Al-Naser [21] studied numerically the hydromagnetic double diffusive convection in a rectangular enclosure with opposing temperature and concentration gradients. Their cavity and conditions were similar to that of Nishimura [18] but they imposed magnetic field and heat generation. They found that the effect of the magnetic field reduced the heat transfer and fluid circulation within the enclosure. Also, they concluded that the average Nusselt number increased owing to the presence of a heat sink while it decreased when a heat source was present. They reported that the periodic oscillatory behaviour in the stream function inherent in the problem was decayed by the presence of the magnetic field. This decay in the transient oscillatory behaviour was speeded up by the presence of a heat source. Chamkha and Al-Naser [22] extended their previous work by changing the boundary conditions of vertical walls to be at constant heat and mass fluxes.

Teamah [23] made a parametric study and an extension for Chamkha and Al-Naser [21,22] study. A range for thermal Rayleigh number is studied from 10^3 to 10^6. This range covers most of the engineering and industrial applications. In addition, a strong magnetic field required for modern electronic devices is considered in this study. For this reason the Hartmann number is increased to 200. Also, the heat generation and absorption coefficients ranged from -50 to $+25$. Moreover, the buoyancy ratio varied from -10 to $+10$. The numerical results are reported for the effect of thermal Rayleigh number and the Hartmann number on the contours of streamline, temperature, and concentration.

In addition, Ma [24] also made an extension for Chamkha and Al-Naser [21] study by developing a temperature–concentration lattice Bhatnagar–Gross–Krook (TCLBGK) model, with a robust boundary scheme for simulating the two-dimensional, hydromagnetic, double-diffusive convective flow of a binary gas mixture in a rectangular enclosure. The numerical results were found to be in good agreement with those of Chamkha and Al-Naser [21].

From the previous review the steady, laminar, hydromagnetic, double-diffusive natural convection flow inside an inclined rectangular enclosure in the presence of heat generation or absorption was not explained. Because this situation is of fundamental interest and because it can have various possible applications such as crystal growth, geothermal reservoirs, nuclear fuel debris removal and solidification of metal alloys, it is of special interest to consider it in the present work. The top and bottom walls of the enclosure are assumed adiabatic and impermeable to mass transfer while the vertical walls are maintained at constant heat and mass fluxes. The cavity is considered with a wide range of inclination of $0^\circ \leqslant \gamma \leqslant 180^\circ$. The magnetic Reynolds number is assumed small so that the induced magnetic field will be negligible.

2. Mathematical model

The physical model considered in this paper is shown in Fig. 1. A two-dimensional inclined rectangular enclosure of height, H and width, L is filled with a binary mixture of gas. The longest sides are maintained at constant and uniform different levels of temperatures and concentrations, thus giving arise to double diffusive free convection flow field. The top and bottom surfaces are assumed to be adiabatic and impermeable. The left wall is the source where the mixture diffuses to the right (sink). A uniform and constant magnetic field, B is applied normal to the heated sides of the cavity. The fluid in this enclosure is assumed to be incompressible, Newtonian, heat generating or absorbing and viscous. Both the viscous dissipation and magnetic dissipation are assumed to be negligible. The magnetic Reynolds number is assumed to be so small that the induced magnetic field is neglected. These assumptions lead to the Boussinesq approximation, Eq. (1), with opposite and

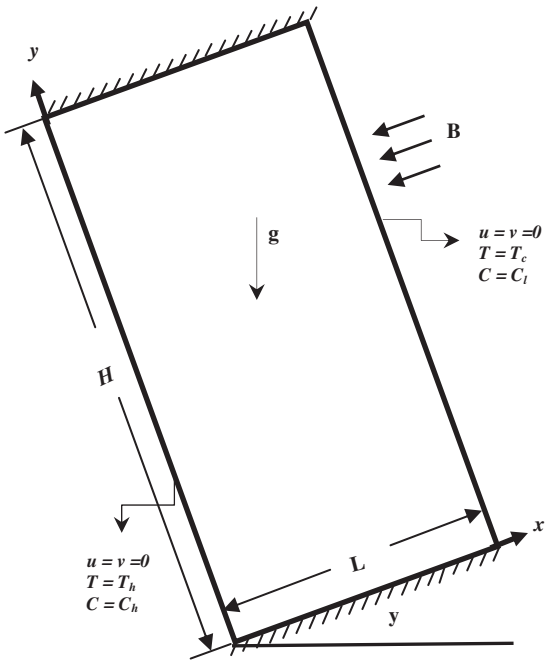

Figure 1 A schematic diagram for the problem with boundary conditions.

compositional buoyancy forces which is used for the body force terms in the momentum equations.

$$\rho = \rho_o[1 - \beta_T(T - T_c) - \beta_S(c - c_l)] \tag{1}$$

The governing equations for the problem under consideration are based on the balance laws of mass, linear momentum, concentration and thermal energy in two dimensions steady state. In the light of assumptions mentioned above, the continuity, momentum, energy and concentration in two dimensional equations can be written as follows:

$$\frac{\partial u}{\partial x} + \frac{\partial v}{\partial y} = 0 \tag{2}$$

$$u\frac{\partial u}{\partial x} + v\frac{\partial u}{\partial y} = -\frac{1}{\rho}\frac{\partial p}{\partial x} + \nu\left[\frac{\partial^2 u}{\partial x^2} + \frac{\partial^2 u}{\partial y^2}\right] + \sin(\gamma)[g\beta_T(T - T_c) - g\beta_s(c - c_l)] \tag{3}$$

$$u\frac{\partial v}{\partial x} + v\frac{\partial v}{\partial y} = -\frac{1}{\rho}\frac{\partial p}{\partial y} + \nu\left[\frac{\partial^2 v}{\partial x^2} + \frac{\partial^2 v}{\partial y^2}\right] + \cos(\gamma)[g\beta_T(T - T_c) - g\beta_s(c - c_l)] - \frac{\sigma B}{\rho} \tag{4}$$

$$u\frac{\partial T}{\partial x} + v\frac{\partial T}{\partial y} = \alpha\left[\frac{\partial^2 T}{\partial x^2} + \frac{\partial^2 T}{\partial y^2}\right] + \frac{Q_o}{\rho C_p}(T - T_c) \tag{5}$$

$$u\frac{\partial c}{\partial x} + v\frac{\partial c}{\partial y} = D\left[\frac{\partial^2 c}{\partial x^2} + \frac{\partial^2 c}{\partial y^2}\right] \tag{6}$$

The boundary conditions for the problem could be written as

- At $x = 0$, $u = v = 0.0$, $T = T_\mathrm{h}$ and $c = c_\mathrm{h}$
- At $x = L$, $u = v = 0.0$, $T = T_\mathrm{c}$ and $c = c_\mathrm{l}$
- And at $y = 0$ and $y = H$;

$$u = v = \frac{\partial T}{\partial y} = \frac{\partial c}{\partial y} = 0 \tag{7}$$

The boundary conditions and the governing equations are non dimensionalized using the following dimensionless variables

$$X = \frac{x}{L}, Y = \frac{y}{L}, U = \frac{uL}{\alpha}, v = \frac{vL}{\alpha}, P = \frac{pL^2}{\rho^*\alpha^2},$$
$$\theta = \frac{T - T_c}{T_h - T_c} \text{ and } C = \frac{c - c_l}{c_h - c_l} \tag{8}$$

After employing the dimensionless variables mentioned above, the resulting dimensionless governing equations can be written as

$$\frac{\partial U}{\partial X} + \frac{\partial V}{\partial Y} = 0 \tag{9}$$

$$U\frac{\partial U}{\partial X} + V\frac{\partial U}{\partial Y} = -\frac{\partial P}{\partial X} + \mathrm{Pr}\left[\frac{\partial^2 U}{\partial X^2} + \frac{\partial^2 U}{\partial Y^2}\right] + \sin(\gamma) \times [\mathrm{Ra}_T\mathrm{Pr}(\theta - NC)] \tag{10}$$

$$U\frac{\partial V}{\partial X} + V\frac{\partial V}{\partial Y} = -\frac{\partial P}{\partial Y} + \mathrm{Pr}\left[\frac{\partial^2 V}{\partial X^2} + \frac{\partial^2 V}{\partial Y^2}\right] + \cos(\gamma) \times [\mathrm{Ra}_T\mathrm{Pr}(\theta - NC)] + \mathrm{Ha}^2\mathrm{Pr} \times V \tag{11}$$

$$U\frac{\partial \theta}{\partial X} + V\frac{\partial \theta}{\partial Y} = \left[\frac{\partial^2 \theta}{\partial X^2} + \frac{\partial^2 \theta}{\partial Y^2}\right] + \phi \times \theta \tag{12}$$

$$U\frac{\partial C}{\partial X} + V\frac{\partial C}{\partial Y} = \frac{1}{\mathrm{Le}}\left[\frac{\partial^2 C}{\partial X^2} + \frac{\partial^2 C}{\partial Y^2}\right] \tag{13}$$

where, Pr is the Prandtl number, $\mathrm{Ra_T}$ is the thermal Rayleigh number, N is the buoyancy ratio $= \beta_\mathrm{s}[(c_\mathrm{h} - c_\mathrm{l})]/\beta_\mathrm{T}[(T_\mathrm{h} - T_\mathrm{c})]$, Ha is the Hartmann number $= \mathrm{BL}\sqrt{\sigma/\mu}$, Φ is the dimensionless heat generation or absorption coefficient $= (Q_\mathrm{o}L^2)/(\rho c_\mathrm{P}\alpha)$, and Le is the Lewis number, $\mathrm{Le} = \alpha/D$

The dimensionless boundary conditions become

- At $X = 0$, $U = V = 0.0$, $\theta = 1$ and $C = 1$
- At $X = 1$, $U = V = 0.0$, $\theta = C = 0$
- And at $Y = 0$ and $Y =$ aspect ratio

$$U = V = \frac{\partial \theta}{\partial Y} = \frac{\partial C}{\partial Y} = 0 \tag{14}$$

The Nusselt and Sherwood numbers calculated as average values and evaluated along the isothermal walls of the cavity are given by

$$\mathrm{Nu} = -\frac{1}{\mathrm{A}}\int_0^A \left(\frac{\partial \theta}{\partial X}\right)_{X=0} \mathrm{dY} \tag{15}$$

$$\mathrm{Sh} = -\frac{1}{\mathrm{A}}\int_0^A \left(\frac{\partial C}{\partial X}\right)_{X=0} \mathrm{dY} \tag{16}$$

3. Numerical method

Numerical solutions of the full conservation equations are obtained using the finite volume technique developed by Patankar [25]. This technique is based on the discretization of the governing equations using the central difference in space.

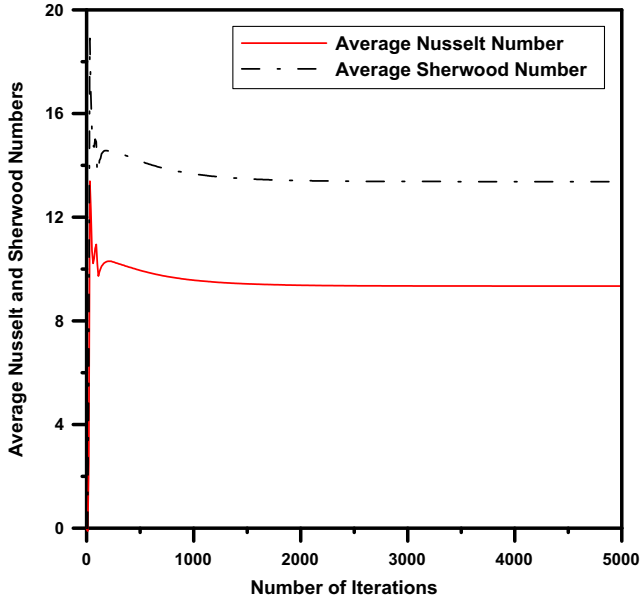

Figure 2 Convergence and stability of the solution Pr = 0.7, $N = 1$, Le = 1, Ha = 10, $\gamma = 60°$, Ra = $10^5$and $\phi = 1$.

Firstly, the number of nodes used was checked. During the program tests (22×62) and (82×242) grids were used. Because of minor differences (less than 0.15%) the results presented here are obtained using number of grids (42×122). The 42 grid points in X-direction were enough to resolve the thin boundary layer near the vertical walls. To calculate both Nusselt and Sherwood numbers, the following numerical differentiations are used, $\frac{\partial\theta}{\partial x}\big|_{X=0}$ *and* $\frac{\partial\theta}{\partial x} = lim_{\Delta X \to 0}\left(\frac{\Delta\theta}{\Delta x}\right)$. Therefore, at the isothermal wall very fine grids are needed to obtain accurate results. In X-direction, the width of 5 control volumes close to both the vertical boundaries were 1/4 the width of the central control volumes. Also the bottom and top surfaces are assumed adiabatic and impermeable. Therefore in Y-direction, numerical differentiations are not needed. Therefore, the height of 5 control volumes close to both the horizontal boundaries were 1/4 the height of the central control volumes.

The discretization equations were then solved by the Gauss–Seidel method. The iteration method used in this program is a line-by-line procedure, which is a combination of the direct method and the resulting Tri Diagonal Matrix Algorithm (TDMA).

In order to check the convergence of the iteration, the change in the average Nusselt and Sherwood numbers as well as other dependent variables through one hundred iterations were checked. Fig. 2 shows that the change in the average Nusselt and Sherwood numbers is less than 0.01% from their initial values which is an indication for the convergence and stability of the solution.

4. Validation

Prior to calculations, checks were conducted to validate the calculation procedure by performing simulation for; double-diffusive convection flow in a vertical rectangular enclosure with combined horizontal temperature and concentration gradients and in the presence of magnetic field and heat generation effects which was reported by Chamkha and Al-Naser [21], numerical simulation of double diffusive natural convection in rectangular enclosure in the presence of magnetic field and heat source which was reported by Teamah [23] and lattice BGK simulations of double diffusive natural convection in a rectangular enclosure in the presence of magnetic field and heat source which was reported by Ma [24].

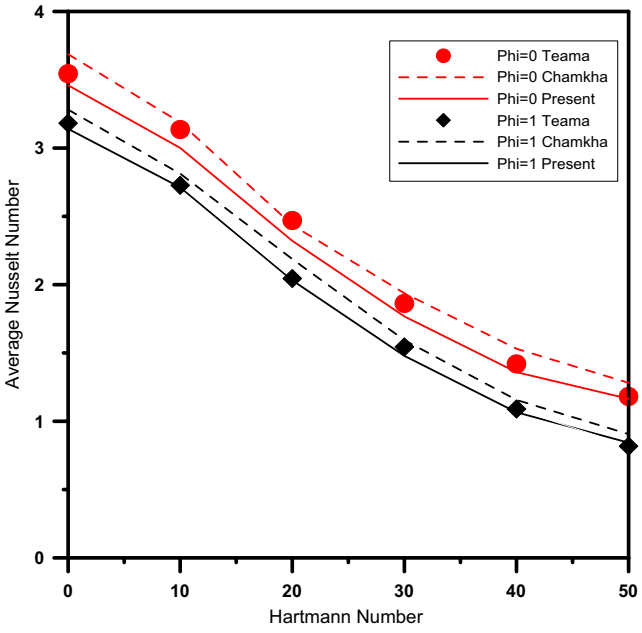

Figure 3 Comparison for average Nusselt number with Chamkha and Al-Naser [21] and Teamah [23] results, $N = 0.8$, Ra = 10^5, Pr = 1, $A = 2$, $\gamma = 0°$ and Le = 2.

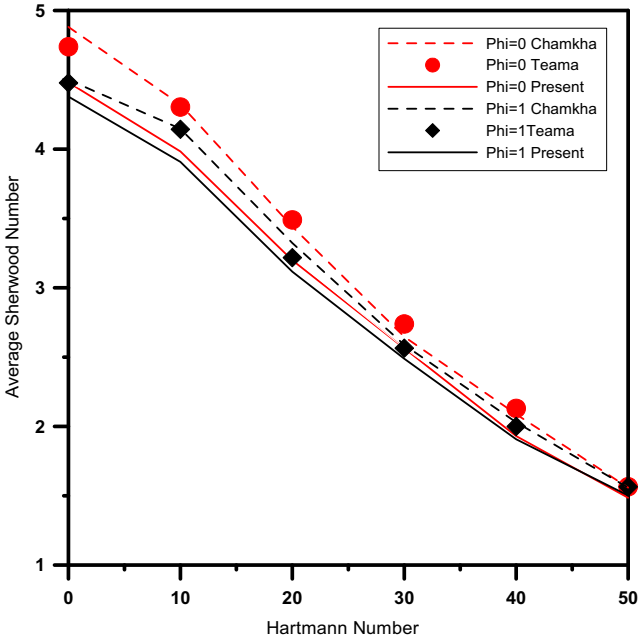

Figure 4 Comparison for average Sherwood number with Chamkha and Al-Naser [21] and Teamah [23] results, $N = 0.8$, Ra = 10^5, Pr = 1, $A = 2$, $\gamma = 0°$ and Le = 2.

Firstly, a comparison for the predicted values for the average Nusselt numbers over a range for Hartmann from 0 to 50 for the present solution and the results published by Chamkha and Al- Naser [21] and Teamah [23] is given in Fig. 3. The following parameters are kept constant; $N = 0.8$, $Ra = 10^5$, $Pr = 1$, $A = 2$, $\gamma = 0°$ and $Le = 2$. The heat generation coefficient equal to zero or one. In addition, Fig. 4 plots the values of the average Sherwood number for the same previous conditions. The maximum deviation between the results through this range was within two percent. Some of this deviation may be

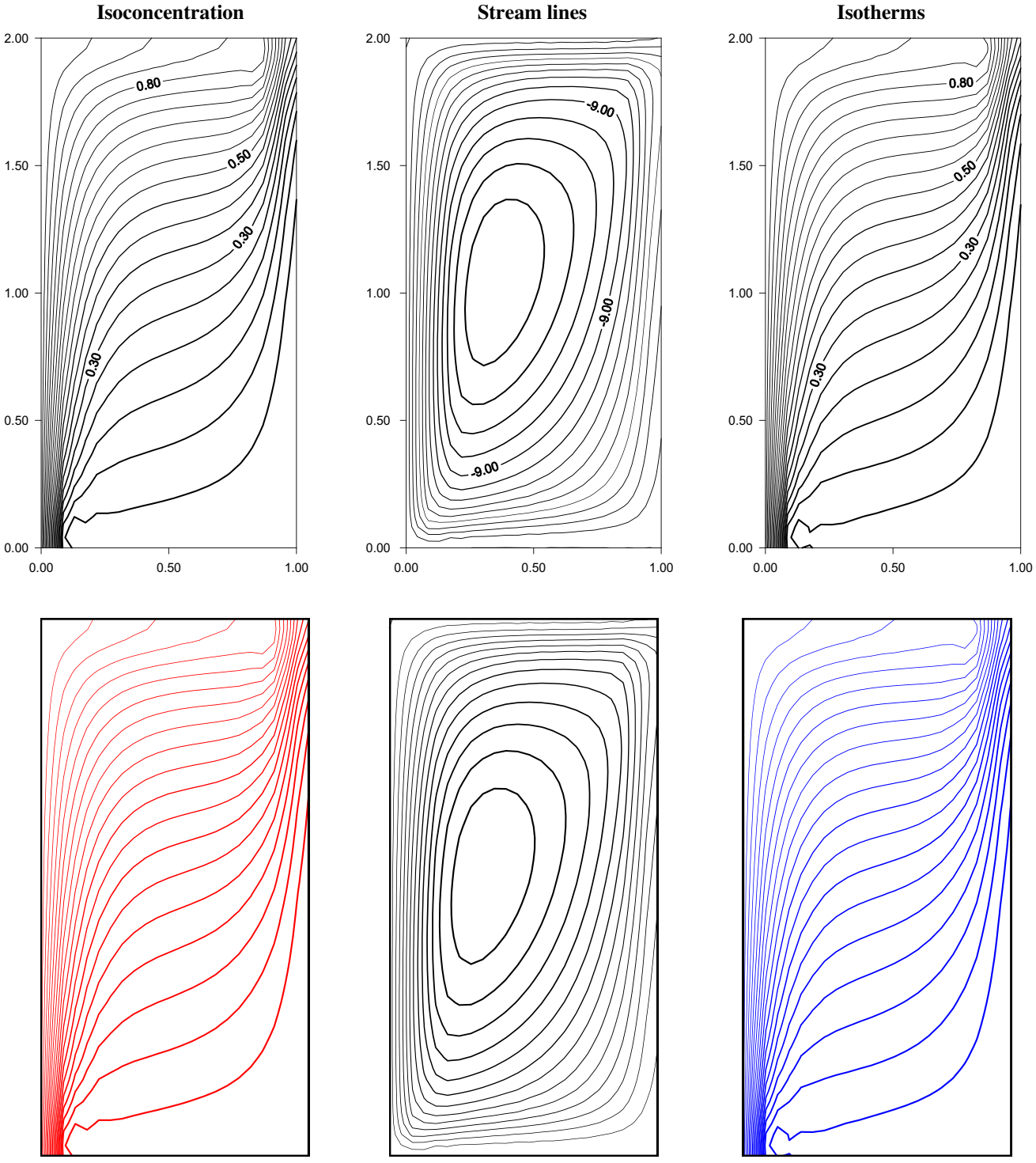

Figure 5 The streamlines, isothermals and isoconcentration contours with $Ha = 100$, $Ra = 10^6$, $Pr = 0.7$, $N = 1$, $Le = 1$, $\gamma = 0°$ and $\phi = 1$ (a) Teamah [23] (b) Present Code.

from the accuracy in the measuring from the graphs or from the solution techniques.

Furthermore, another validation for the present numerical solution is done by making comparisons for the isotherms, concentration and streamlines contours of the present work with previous work. Fig. 5 is a comparison for the isotherms, concentration and streamlines contours of the present work and Teamah [23] with the following parameters kept constant;

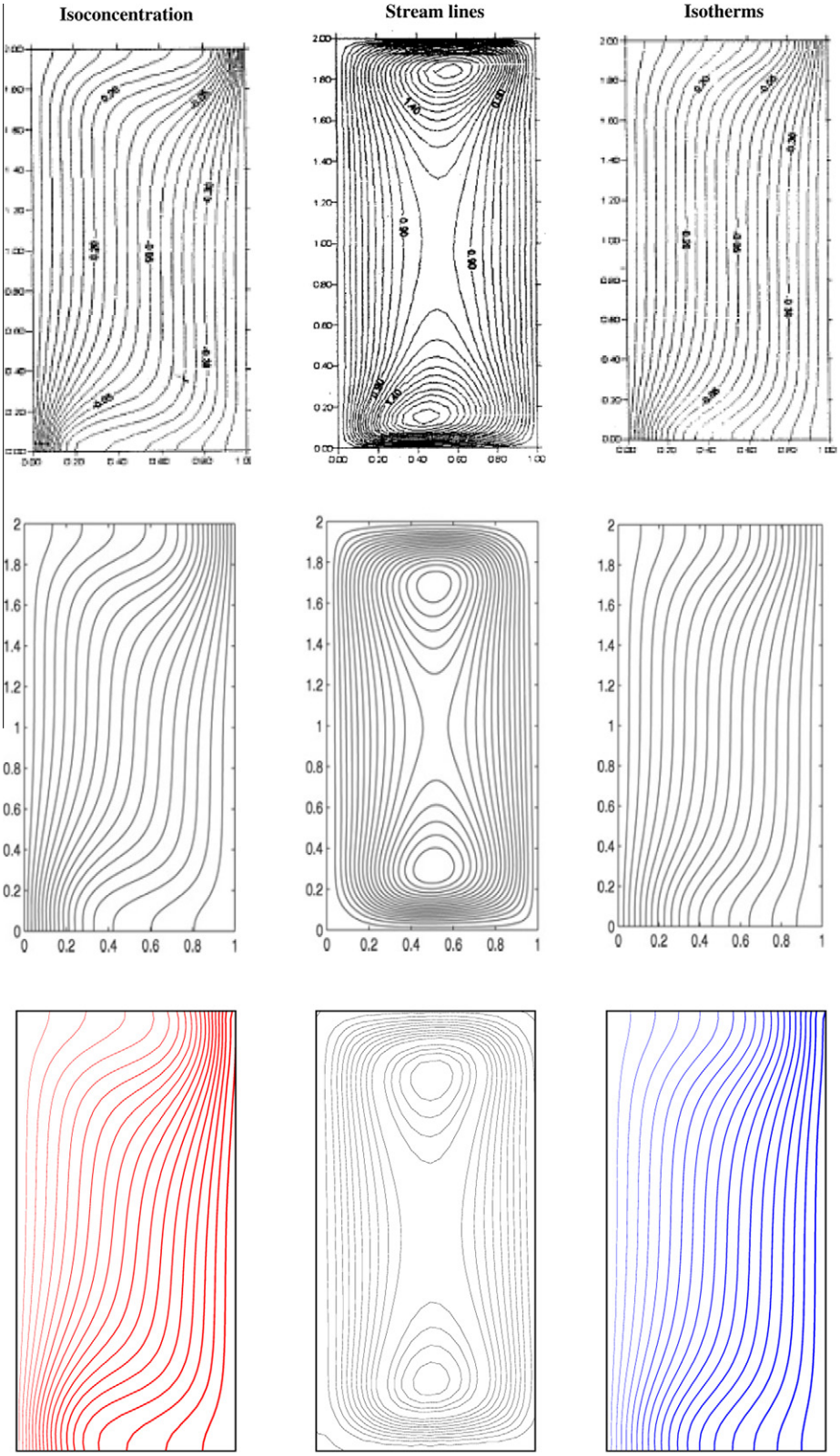

Figure 6 The streamlines, isothermals and isoconcentration contours with Ha = 50, Ra = 10^5, Pr = 1, Le = 2, $N = 0.8$, $\gamma = 0°$ and $\phi = 0$ (a) Chamkha and El-Naser [21] (b) Ma [24] (c) Present Code.

Ha = 100, Ra = 10^6, Pr = 1, Le = 2, $\gamma = 0°$ and $\phi = 1$. Finally, Fig. 6 is a comparison for the isotherms, concentration and streamlines contours of the present work and Chamkha and Al-Naser [21] and Ma [24] with the following parameters kept constant; Ha = 50, Ra = 10^5, Pr = 1, Le = 2, $\gamma = 0°$ and $\phi = 0$. Figs. 5 and 6 both show good agreement.

5. Results and discussions

The governing parameters in the double diffusive natural convection in an inclined rectangular enclosure in the presence of magnetic field and heat source are the Prandtl number, Pr; the Lewis number, Le; the Rayleigh number, Ra_T; the Hartmann number, Ha; the buoyancy ratio, N; the dimensionless heat generation or absorption coefficient, Φ and the inclination angle, γ. In the present study, the Prandtl number, Pr is kept constant at Pr = 0.7, aspect ratio, $A = 2$, Lewis number, Le = 2, the buoyancy ratio, $N = 1$, the Hartmann number, Ha = 10 and the dimensionless heat generation, $\Phi = 1$. Computations are carried out for Ra_T ranging from 10^3 to $5 * 10^5$ and inclination angle range of $0° \leqslant \gamma \leqslant 180°$. The numerical results for the streamlines, isothermals and isoconcentration contours for various values of thermal Rayleigh number Ra_T, will be presented and discussed for different inclination angles. In addition, the effect of the Rayleigh number on the average Nusselt and Sherwood numbers at various conditions will also be presented and discussed.

5.1. Combined effect of thermal Rayleigh number and inclination angle on the streamlines, isotherms and isoconcentrations contours

Fig. 7 shows the effect of thermal Rayleigh number on the streamlines, isotherms and isoconcentrations contours for inclination angles; $\gamma = 0°$, 45°, 90°, 135° and 180° with the following parameters kept constants; Le = 2, Ha = 10, Pr = 0.7, $N = 1$ and $\phi = 1$.

For low thermal Rayleigh number values ($Ra = 10^3$) the conduction regime is dominant in all the cavities as shown in Fig. 7a. The isotherms and isoconcentration lines are almost parallel lines to the isothermal walls indicating that most heat transfer is by conduction. The effect of heat generation is observed as it opposes the heat flow from hot wall. Moreover, the cold wall receives much heat than that input by the hot one. Therefore, near the hot wall, the value of temperature gradient is less than that near the cold wall. In addition, the flow consists of a very weak clockwise rotating cell (one unicell) with maximum strength $\psi_{max} = 1.6$. Since, the cell is coming to the hot wall from the cavity bottom and departs from it at the cavity top, both heat and mass transfer at the cavity bottom is higher than at the top. Also, it is seen from Fig. 7a that the isothermals and isoconcentrations are closer to the hot wall in the lower region. In addition, the effect of thermal Rayleigh number on the streamline, isothermals and isoconcentration contours for the horizontal cavity (heated from below) is quite different from other cavities. The flow field does not consist of uni-cellular flow as the other cavities but it consists of two-cellular flows (Benard cellular flow) with each cell rotating along the opposite direction. The fluid near the lower wall (the hot wall) has lower density and it needs to move upwards while on the other hand the fluid near the upper wall (the cold wall) needs to move downwards. This causes the cavity to be divided into two squares each with a unicellular flow rotating along the opposite direction to its neighboring ones with $\psi_{max} = 0.022$.

The contribution of convection is noticeable at high Rayleigh number as evident by the departure of the isotherms from the vertical pattern and the mechanism of heat transfer is gradually shifted to natural convection. The contours plots of concentration are more inclined than this of temperature, which is due to higher heat rate, 1/Le, with Le > 1. Fig. 7b plots the contours at Rayleigh number ($Ra = 5 * 10^3$) where convection

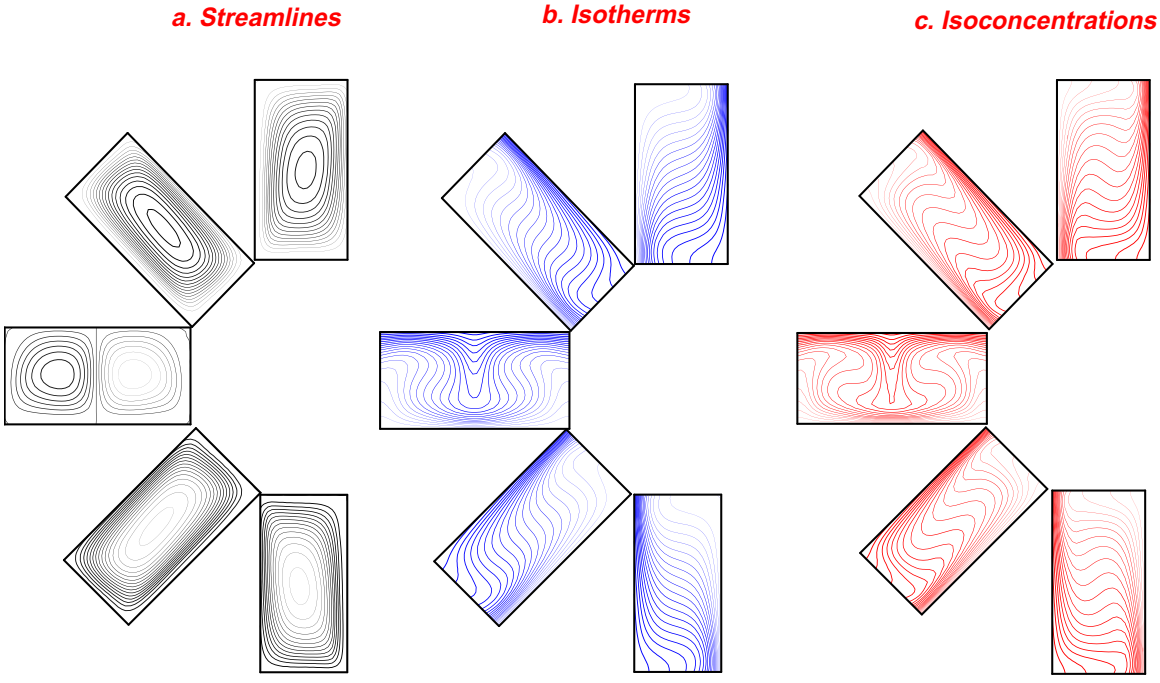

Figure 7a The streamlines, isothermals and isoconcentration contours with Ha = 10, Pr = 0.7, Le = 2, $N = 1$, $\phi = 1$ and $Ra = 10^3$.

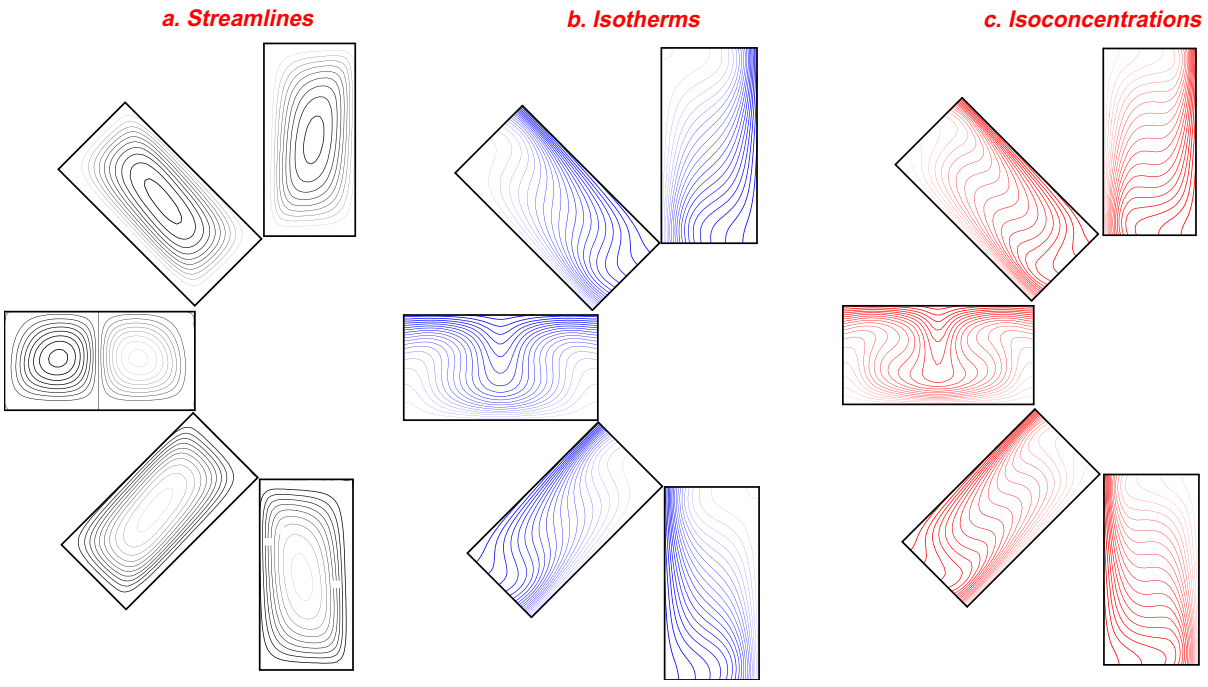

Figure 7b The streamlines, isothermals and isoconcentration contours with Ha = 10, Pr = 0.7, Le = 2, $N = 1$, $\phi = 1$ and Ra = $5 * 10^3$.

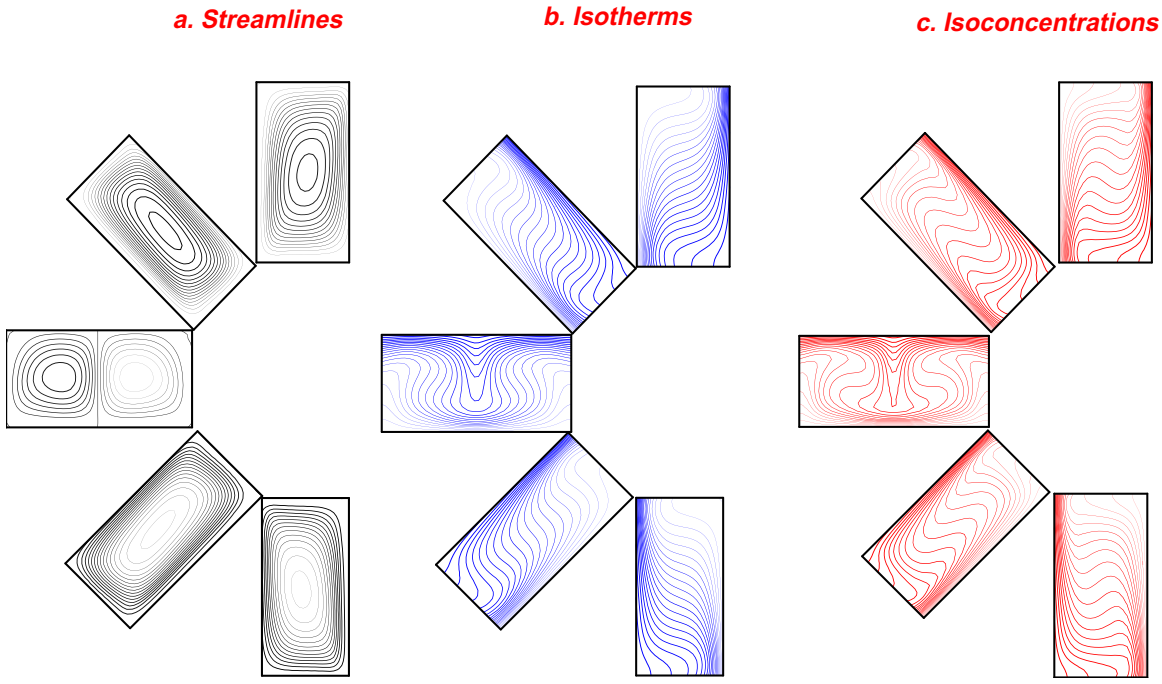

Figure 7c The streamlines, isothermals and isoconcentration contours with Ha = 10, Pr = 0.7, Le = 2, $N = 1$, $\phi = 1$ and Ra = 10^4.

is more pronounced and the flow cell moves upward and its strength increases. The maximum strength of the rotating cell is $\psi_{max} = 5$ for the upwards and downwards cavities, $\psi_{max} = 5.5$ for the inclined cavity at $\gamma = 45°$ and the inclined cavity at $\gamma = 135°$. The maximum strength for the horizontal cavity is $\psi_{max} = 4.5$ which is located at the centre of the cavity. This is clarified by the fact that the isotherms and isoconcentrations are closer to the hot wall in the middle region and subsequently the heat and mass transfer are maximum at this region.

Moreover, Fig. 7c plots the contours at Rayleigh number (Ra = 10^4). The strength of flow cells is higher than Fig. 7b. The maximum strength; $\psi_{max} = 7$ for the upwards and downwards cavities, $\psi_{max} = 8$ for the inclined cavity at

$\gamma = 45°$ and the inclined cavity at $\gamma = 135°$. This is an indication for higher convection current within the cavity. The isotherms and isoconcentrations are further shifting to the horizontal distribution in the cavity core.

Further increase in Rayleigh number to $Ra = 5 * 10^4$ and 10^5 as shown in Fig. 7d and e causes distortion in the central flowing cell. The maximum strength for the flowing cell in Fig. 7d is $\psi_{max} = 16$ for the upwards and downwards cavities, $\psi_{max} = 15$ for the inclined cavity at $\gamma = 45°$ and the inclined cavity at $\gamma = 135°$. The streamlines are crowded near the cavity wall and the cavity core is empty. In addition, two secondary symmetrical rotating cells developed in the streamlines contours of the horizontal cavity. The circulation within the horizontal cavity has maximum strength of $\psi_{max} = 1.6$. The

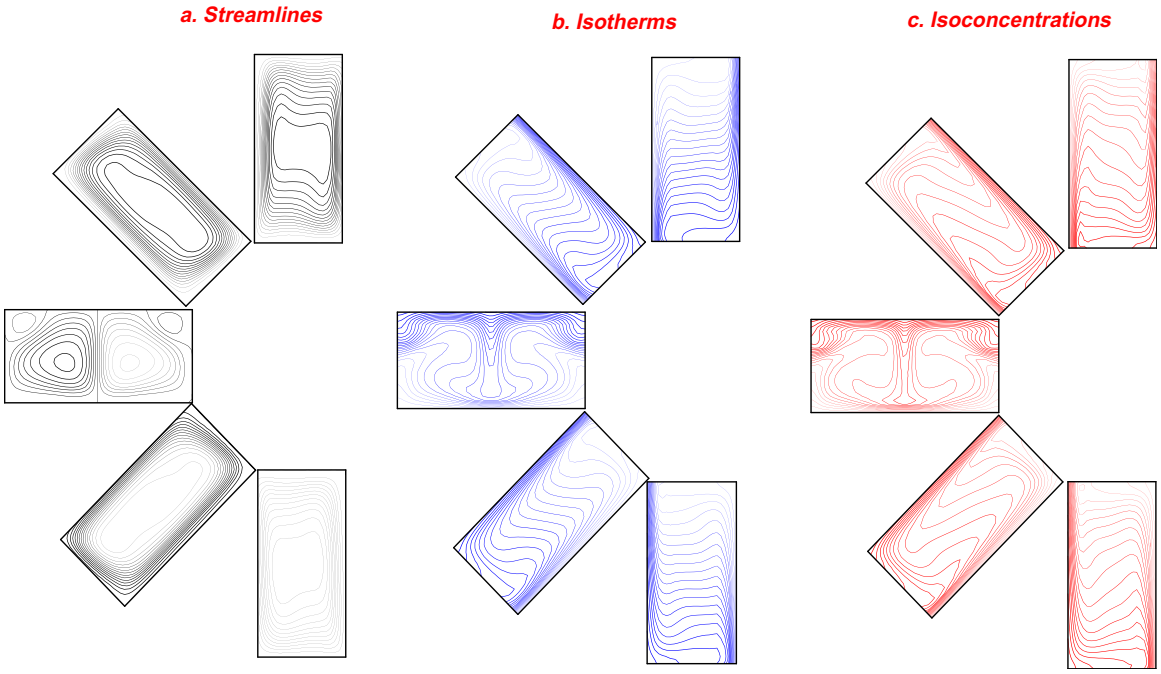

Figure 7d The streamlines, isothermals and isoconcentration contours with Ha = 10, Pr = 0.7, Le = 2, $N = 1$, $\phi = 1$ and $Ra = 5 * 10^4$.

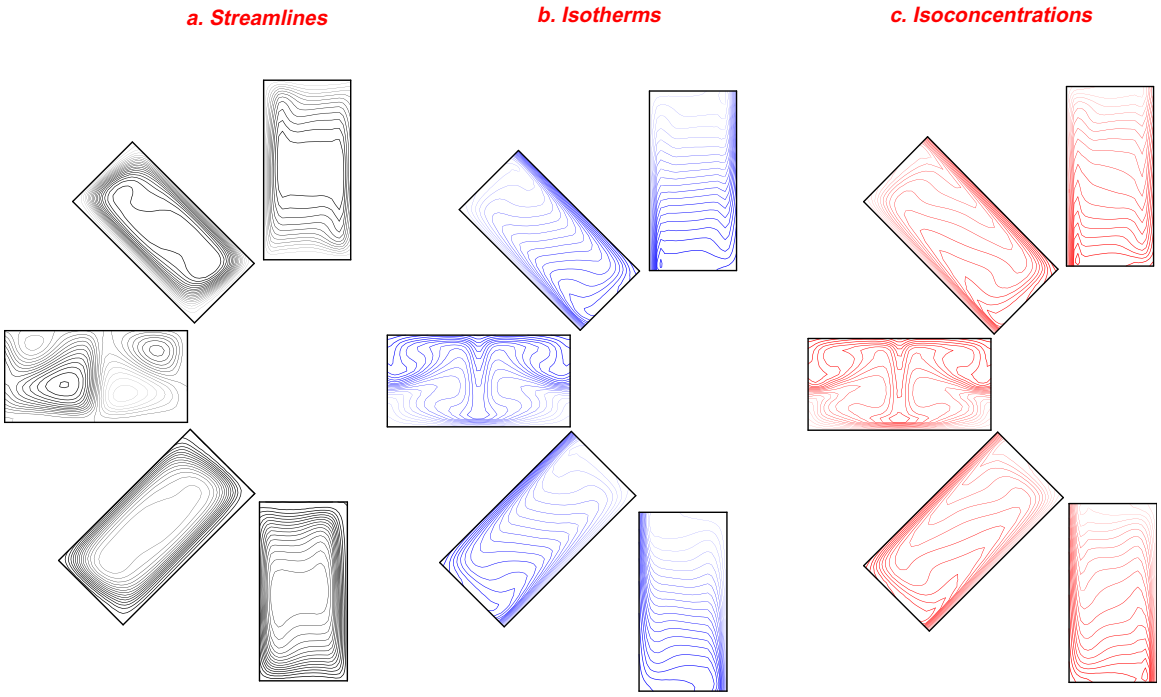

Figure 7e The streamlines, isothermals and isoconcentration contours with Ha = 10, Pr = 0.7, Le = 2, $N = 1$, $\phi = 1$ and $Ra = 10^5$.

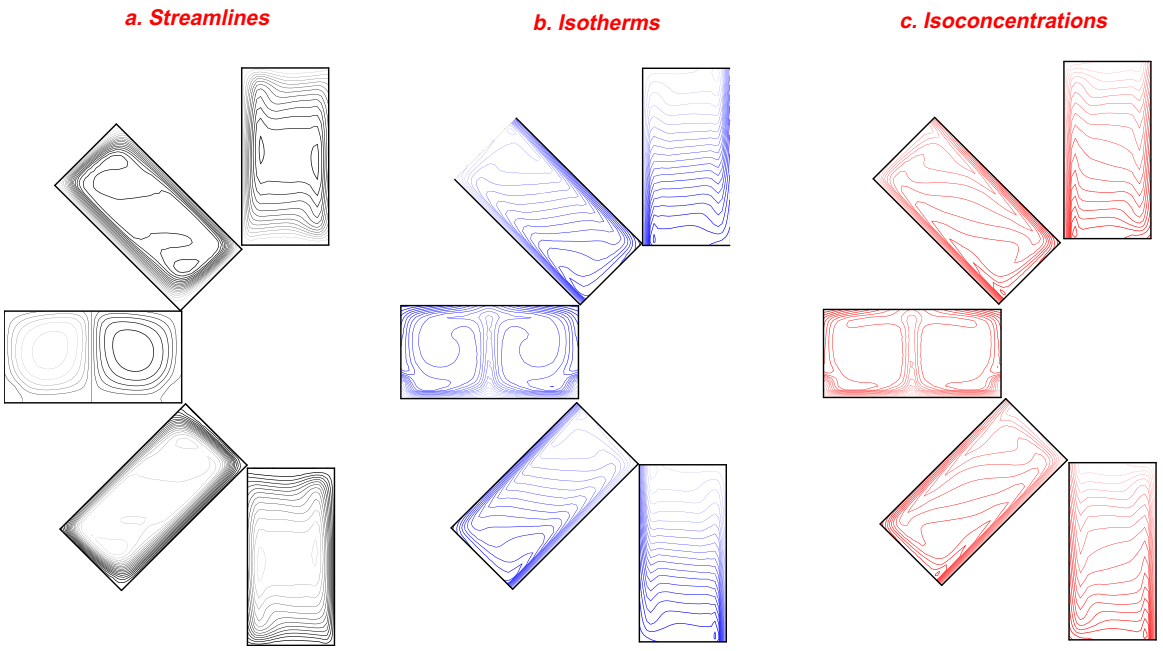

Figure 7f The streamlines, isothermals and isoconcentration contours with Ha = 10, Pr = 0.7, Le = 2, $N = 1$, $\phi = 1$ and Ra = $5 * 10^5$

isotherms and isoconcentrations are further shifting to the horizontal position as Rayleigh number increases. But the isotherms and isoconcentration of the horizontal cavity show similar configurations to the case of Ra = $5 * 10^3$ but with further stratifications in the centre of the cavity.

Additionally, similar contribution for high thermal Rayleigh number is also noticed in Fig. 7e. The flow cell strength further increases with maximum strength; $\psi_{max} = 26$ for the upwards and downwards cavities, $\psi_{max} = 20$ for the inclined cavity at $\gamma = 45°$ and the inclined cavity at $\gamma = 135°$. In addition, multiple secondary rotating cells developed in the upper corners of the horizontal cavity. The circulation in the horizontal cavity increases reaching $\psi_{max} = 26$. Similar distributions for the isotherms and isoconcentrations contours to Fig. 7d occur in Fig. 7e.

For even higher values of Ra = $5 * 10^5$, Fig. 7f shows that the isotherms and isoconcentration are almost parallel lines to the isothermal walls. Also, the isotherms and isoconcentration are in the thin boundary layer and stratified in the core of the cavity.

This can be attributed to high convection current within the cavity which also causes a reduction in the temperature gradient in the centre of the cavity. The strength of the flowing cell increases with $\psi_{max} = 26$ for the upwards and downwards cavities, $\psi_{max} = 34$ for the inclined cavity at $\gamma = 45°$ and the inclined cavity at $\gamma = 135°$ and $\psi_{max} = 60$ for the horizontal cavity.

5.2. Effect of inclination on the local Nusselt and Sherwood numbers

Fig. 8a and b illustrates the effect of inclination on the local Nusselt and Sherwood numbers over the hot wall with the following parameters kept constant; Le = 2, Ha = 10, Pr = 0.7, $N = 1$, Ra = 10^4, $\phi = 1$ and $\gamma = 0°$, 45°, 90°, 135° and 180°.

As shown in Fig. 8a, for the vertical cavity and the cavity inclined at $\gamma = 45°$, the local Nusselt number has maximum values at the cavity bottom and its value decreases as we move upwards. If we return to Fig. 7c the absolute value for the temperature gradient has maximum value at the bottom of these cavities and minimum values at the cavities top. The opposite contribution is for the cavities inclined at $\gamma = 135°$ and 180°, where the local Nuselt number has minimum values at the

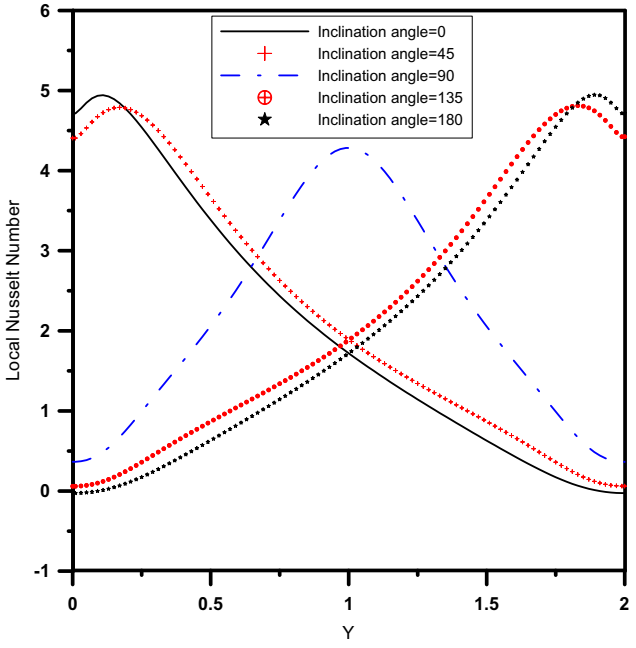

Figure 8a The local Nusselt number versus Y, with Ha = 10, Pr = 0.7, Le = 2, $N = 1$, $\phi = 1$, Ra = 10^4 and $\gamma = 0°$, 45°, 90°, 135° and 180°.

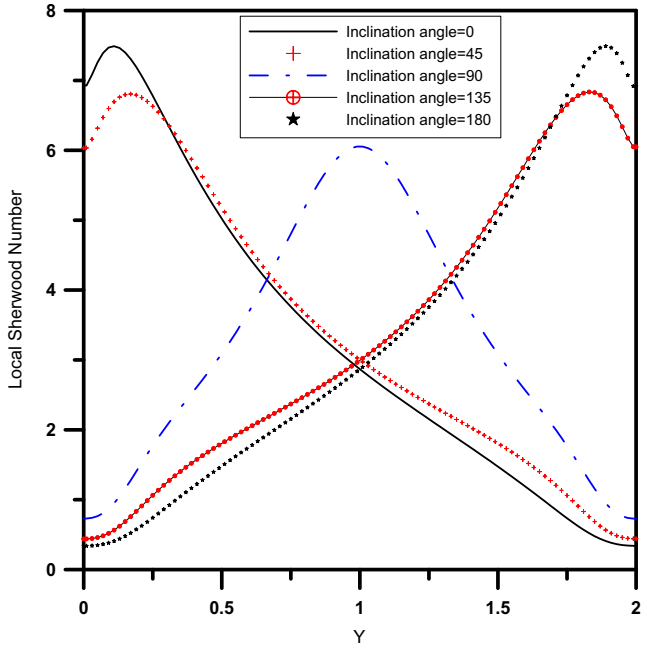

Figure 8b The local Sherwood number versus Y, with Ha = 10, Pr = 0.7, Le = 2, $N = 1$, $\phi = 1$, Ra = 10^4 and $\gamma = 0°$, 45°, 90°, 135° and 180°.

cavity bottom and its value increases as we move upwards. Also this is clarified by referring to Fig. 7c where the absolute value for the temperature gradient has minimum value at the bottom of these cavities and maximum values at the cavities top. In addition, the horizontal cavity experiences different behavior. The local Nusselt number has minimum values at the cavity bottom which then starts to increase as we move upwards until it has maximum value at the cavity center ($Y = 1$). Then the local Nusselt number starts to decrease once again reaching its initial value at the cavity top. Fig. 7c emphasizes this behavior of the local Nusselt number for the horizontal cavity. The absolute value for the temperature gradient has minimum value at the bottom of the cavity and it starts to increase as we move upwards reaching the maximum value at the centre of the cavity and then decreases once again reaching the initial minimum values at the cavity top. Furthermore, Fig. 8b shows the local Sherwood number over the hot wall. Similar contributions to Fig. 8a are obtained but with higher values for the local Sherwood number. Finally, referring to Fig. 8a and b it is clarified that the highest values for the local Nusselt and Sherwood numbers are at the cavities inclined at $\gamma = 45°$ and 135°.

5.3. Effect of thermal Rayleigh number on the average Nusselt and Sherwood numbers

Fig. 9a and b illustrates the effect of thermal Rayleigh number on the average Nusselt and Sherwood numbers for inclination angle range of $0° \leqslant \gamma \leqslant 180°$. Fig. 8a shows that generally for all inclination angles, as Rayleigh number increases the average Nusselt number increases. For the horizontal cavity, $\gamma = 90°$, at lower values of Rayleigh number, Ra = 10^3, the average Nusselt number has the lowest value in comparison with other cavities. This is clarified by referring to the isotherms contours in Fig. 7a where the isotherms are parallel lines and hence the conduction regime is highly dominant compared to other cavities. For $10^3 < \text{Ra} < 5 * 10^4$, the average Nusselt number of the horizontal cavity has the maximum value when compared to other cavities. This is also clarified by referring to the isotherms in Fig. 7b and c where the isotherms of the horizontal cavity are closely attached to the heated wall in the middle region over a larger distance when compared to

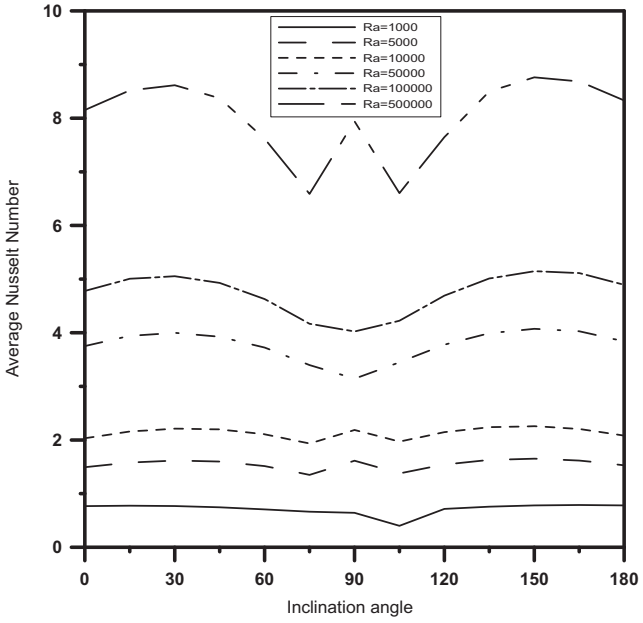

Figure 9a The effect of thermal Rayleigh number on the average Nusselt number for inclination angle range of $0° < \gamma < 180°$.

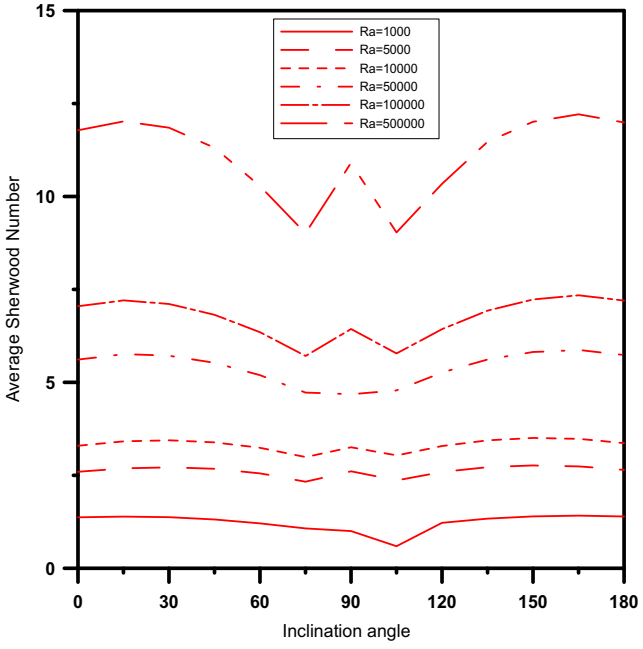

Figure 9b The effect of thermal Rayleigh number on the average Sherwood number for inclination angle range of $0° < \gamma < 180°$.

the other cavities. This means that $\left(\frac{\partial\theta}{\partial X}\right)\text{at}X=0$ (along the heated wall) has larger values when compared to other cavities and hence larger average Nusselt number. In addition, for $5*10^4 \leqslant \text{Ra} < 5*10^5$, the average Nusselt number of the horizontal cavity starts to decrease unlike other cavities. This behavior is clarified by again referring to the isotherms contours in Fig. 7d and e. The isotherms are closely attached to the heated wall in smaller areas and subsequently the average Nusselt number decreases. Finally, for higher values of Rayleigh number $\text{Ra} = 5*10^5$, it is expected that the average Nusselt number for the horizontal cavity decreases but the opposite occurred due to the high instabilities that occur in the case of cavities heated from below (Rayleigh Benard instability).

Fig. 9b shows similar consequences for the effect of Rayleigh number on the average Sherwood number for the same range of inclination angles. The values of the average Sherwood number are higher than those of the average Nusselt number. Also, generally for all inclination angles as Rayleigh number increases the average Sherwood number increases. The exception is for the horizontal cavity as mentioned above. Over the range of $10^3 \leqslant \text{Ra} \leqslant 5*10^4$ the same results of the average Nusselt number are applied here for the average Sherwood number. In contrast, the instabilities started to appear earlier at $\text{Ra} = 10^5$ and continued for even higher values of Rayleigh number $\text{Ra} = 5*10^5$. In conclusion, referring to Fig. 9a and b, it is clarified that the highest values of the average Nusselt and Sherwood number are at the cavities inclined at $\gamma = 45°$ and 135°.

6. Conclusion

Steady heat and mass transfer by natural convection flow of a heat generating fluid inside an inclined rectangular enclosure in the presence of a transverse magnetic field was studied numerically. The finite-difference method was employed for the solution of the present problem. Comparisons with previously published work on special cases of the problem were performed and found to be in good agreement. Graphical results for various parametric conditions were presented and discussed. It was found that the heat and mass transfer mechanisms and the flow characteristics inside the enclosure depended strongly on the thermal Rayleigh number. Increasing the source term in the momentum equation, by increasing the Rayleigh number, always lead to increases on the heat and mass transfer performance of the enclosure. This is clarified by plotting the average Nusselt and Sherwood numbers with different values of thermal Rayleigh number and for different inclination angles. Also, the different flow characteristics of the horizontal cavity were discussed in details (Rayleigh–Benard convection). Furthermore, results revealed that the best inclination angles are $\gamma = 45°$ and 135° since both cases have higher values of local and average Nusselt and Sherwood numbers.

References

[1] G. de Vahl Davis, Laminar natural convection in an enclosed rectangular cavity, Int. J. Heat Fluid Flow 11 (1968) 1675–1693.

[2] S. Acharya, R.J. Goldstein, Natural convection in an externally heated square box containing internal energy sources, J. Heat Transfer 107 (1985) 855–866.

[3] M. Rahman, M.A.R. Sharif, Numerical study of laminar natural convection in inclined rectangular enclosures of various aspect ratios, Numer. Heat Transfer, Part A 44 (2003) 355–373.

[4] Abdalla AlAmiri, Khalil Khanafer, Ioan Pop, Buoyancy-induced flow and heat transfer in a partially divided square enclosure, Int. J. Heat Mass Transfer 52 (2009) 3818–3828.

[5] H. Oztop, E. Bilgen, Natural convection in differentially heated and partially divided square cavities with internal heat generation, Int. J. Heat Fluid Flow 27 (2006) 466–475.

[6] H. Ozoe, K. Okada, The effect of the direction of the external magnetic field on the three-dimensional natural convection in a cubic enclosure, Int. J. Heat Mass Transfer 32 (1989) 1939–1953.

[7] N.I. Wakayama, Behavior of flow under gradient magnetic field, J. Appl. Phys. 69 (4) (1991) 2734–2736.

[8] B. Bai, A. Yabe, J. Qi, N.I. Wakayama, Quantitative analysis of air convection caused by magnetic-fluid coupling, AIAA J. 37 (1999) 1538–1543.

[9] T. Tagawa, R. Shigemitsu, H. Ozoe, Magnetizing force modeled and numerically solved for natural convection of air in a cubic enclosure: effect of the direction of the magnetic field, Int. J. Heat Mass Transfer 45 (2002) 267–277.

[10] M. Kaneda, T. Tagawa, H. Ozoe, Convection induced by a cusp-shaped magnetic field for air in a cube heated from above and cooled from below, J. Heat Transfer 124 (2002) 17–25.

[11] J.L. Morton, N. Ma, D.F. Bliss, G.G. Bryant, Dopant segregation during liquid-encapsulated Czochralski crystal growth in a steady axial magnetic field, J. Cryst. Growth 242 (2002) 471–485.

[12] N. Ma, J.S. Walker, A model of dopant transport during Bridgman crystal growth with magnetically damped buoyant convection, J. Heat Transfer 122 (2000) 159–164.

[13] N. Ma, J.S. Walker, A parametric study of segregation effects during vertical Bridgman crystal growth with an axial magnetic field, J. Cryst. Growth 208 (2000) 757–771.

[14] J.F. Kuniholm, N. Ma, Natural convection in a liquid encapsulated molten semiconductor with a steady magnetic field, Int. J. Heat Fluid Flow 24 (2003) 130–136.

[15] S. Ostrach, Natural convection with combined driving forces, Phys. Chem. Hydrodyn. 1 (1980) 233–247.

[16] V.A.F. Costa, Double diffusive natural convection in a square enclosure with heat and mass diffusive walls, Int. J. Heat Mass Transfer 40 (1997) 4061–4071.

[17] V.A.F. Costa, Double-diffusive natural convection in parallelogrammic enclosures, Int. J. Heat Mass Transfer 47 (2004) 2913–2926.

[18] T. Nishimura, M. Wakamatsu, A.M. Morega, Oscillatory double diffusive convection in a rectangular enclosure with combined horizontal temperature and concentration gradients, Int. J. Heat Mass Transfer 41 (1998) 1601–1611.

[19] R. Chouikh, L. Ben Snoussi, A. Guizani, Numerical study of the heat and mass transfer in inclined glazing cavity: Application to a solar distillation cell, Renewable Energy 32 (2007) 1511–1524.

[20] N. Nithyadevi, Ruey-Jen Yang, Double diffusive natural convection in a partially heated enclosure with Soret and Dufour effects, Int. J. Heat Fluid Flow 30 (2009) 902–910.

[21] A.J. Chamkha, H. Al-Naser, Hydromagnetic double-diffusive convection in a rectangular enclosure with opposing temperature and concentration gradients, Int. J. Heat Mass Transfer 45 (2002) 2465–2483.

[22] A.J. Chamkha, H. Al-Naser, Hydromagnetic double-diffusive convection in a rectangular enclosure with uniform side heat and mass fluxes and opposing temperature and concentration gradients, Int. J. Therm. Sci. 41 (2002) 936–948.

[23] Mohamed A. Teamah, Numerical simulation of double diffusive natural convection in rectangular enclosure in the presences of magnetic field and heat source, Int. J. Therm. Sci. 47 (2008) 237–248.
[24] Changfeng Ma, Lattice BGK simulations of double diffusive natural convection in a rectangular enclosure in the presences of magnetic field and heat source, Nonlinear Anal.: Real World Appl. 10 (2009) 2666–2678.
[25] S.V. Patankar, Numerical Heat Transfer and Fluid Flow, McGraw-Hill, New York, 1980.